RSC Advances

ROYAL SOCIETY OF CHEMISTRY

www.rsc.org/advances

Pd_1/BN as the promising single atom catalyst of CO oxidation: A dispersion-corrected density functional theory study

Zhansheng Lu [a], Peng Lv [a], Jie Xue [a], Huanhuan Wang [a], Yizhe Wang [a], Yue Huang [a], Chaozheng He [b *], Dongwei Ma [c], and Zongxian Yang [a, d*]

[a] *College of Physics and Electronic Engineering, Henan Normal University, Xinxiang 453007, China*

[b] *College of Physics and Electronic Engineering, Nanyang Normal University, Nanyang 473061, China*

[c] *School of Physics, Anyang Normal University, Anyang 455000, China*

[d] *Collaborative Innovation Center of Nano Functional Materials and Applications，Henan Province, China*

Abstract

Single metal atom catalysts exhibit extraordinary activity in a large number of reactions, and some two-dimension materials (such as graphene and h-BN) are found to be the prominent support to stabilize the single metal atom. The CO oxidation reaction on single Pd atom supported by two-dimensional h-BN is investigated systematically by using dispersion-corrected density functional theory study. The great stability of the h-BN supported single Pd atom is revealed, and the single Pd atom prefers to stay at the boron vacancy. Three proposed mechanisms (Eley–Rideal, Langmuir–Hinshelwood, and a "new" termolecular Eley–Rideal) of the CO oxidation were investigated, and two of them (the traditional Langmuir–Hinshelwood mechanism and the new termolecular Eley–Rideal mechanism) are found with the rather small reaction barriers of 0.66 eV and 0.39 eV for their rate-limiting steps, respectively, which suggests that the CO oxidation could proceed at a low temperature on single Pd atom doped h-BN. The current study will help to understand the various mechanisms of the CO oxidation and shed light on the design of the CO oxidation catalyst, especially based on the concept of single metal atom.

* Corresponding authors.
E-mail addresses: hecz2013@nynu.edu.cn(C. He), yzx@henannu.edu.cn (Z. Yang)

1. Introduction

As a kind of the poisonous and harmful gas in the air, the carbon monoxide (CO) catalytic oxidation reaction is of practical importance to phase down its emission from automobiles and industries. So plentiful efforts and studies have been devoted to design more efficient catalysts for this important reaction. As the typical catalysts for CO oxidation, noble metals, such as Au[1], Pt[2-4] and Pd[3, 4] have been widely investigated. Given the low catalytic activities, the poor stabilities and the high cost of the noble metal catalysts, "single metal atom" catalyst proposed by Thomas et al.[5] has sparked worldwide interest in very recent years owing to its great activity and the reduction of its cost.

Experimentally, there is some progress on the concept of "single atom" catalyst (SAC) made through the use of mass-selected soft-landing technique, improved wet chemistry method, or atomic layer deposition method to synthetize the single-atom on various supports[6-8]. The stability of the single atom catalysts is a crucial challenge due to the mobility of the single atom[9]. Fortunately, the practical Pt single atom catalyst supported by iron oxide was experimentally prepared for the first time by Qiao et al. (named as Pt_1/FeO_x), and the excellent performance of the Pt_1/FeO_x demonstrates that heterogeneous catalysis with single atom catalyst is no longer a dream[10]. Moreover, two-dimensional (2D) materials with large specific surface area and great stability, such as graphene, and freestanding hexagonal BN monolayer (h-BN), are found to be prominent catalyst supports to stabilize single metal atoms. For example, single atomic Au on h-BN with boron vacancy exhibits great thermally stability even during the CO oxidation process[11]. And single Ru atom embedded on h-BN is extraordinarily stable because of its dramatically huge diffusion energy barrier[12].

The graphene supported individual, isolated Fe[13], Au[14], Pt[15, 16] and Cu[17] atoms present great activity and selectivity to the CO oxidation reaction. And the h-BN supported single atomic Au[11], Ru[12], Co[18], Cu[19], Pt[20] and Fe[21] promote the CO oxidation at the low temperature. Pd and its alloy, as the typical catalysts for CO oxidation, present high activity[22, 23].

In the current study, as the joint system of Pd and 2D freestanding material, we focus on the stability and activity of the single atomic Pd supported by h-BN (Pd_1-BN) for CO oxidation. The stability of Pd_1-BN will be revealed by the mobility of the single Pd adatom from the calculated diffusion barrier. The entire CO oxidation process on Pd_1-BN is investigated with the various adsorption configurations of CO and O_2 and the different reaction mechanisms of CO oxidation, *via* a new mechanism over the normal bi-molecule Eley–Rideal (ER) and Langmuir–Hinshelwood (LH) mechanisms. Whether and how the single Pd atom could promote the CO oxidation will be focused on. The current study will help to understand the various mechanisms of the CO oxidation and shed light on the design of the CO oxidation catalyst based on the single metal atom concept, and the various catalyst for other reaction based on the single metal atom concept.

2. Methods

All spin-unrestricted calculations were performed within Dispersion-corrected density functional theory DFT (DFT-D) computations as implemented in DMol[3] code embedded in Materials Studio (Accelrys, SanDiego, CA), using a DFT semi-core pseudopotential[24] with GGA-PBE functional[25] with long-range dispersion correction *via* Tkatchenko and Scheffler's scheme[26]. During geometrical optimization, the basis set cut-off was chosen to be 3.5 Å. The convergence tolerances for the geometry optimization were set to 10^{-5} Ha (1 Ha = 27.21 eV) for the energy, 0.002 Ha/Å for the force, and 0.005 Å for the displacement. The electronic SCF tolerance was set to 10^{-6} Ha. In order to achieve accurate electronic convergence, we apply a smearing of 0.005 Ha to the orbital occupation. The reciprocal space was sampled with a (5×5×1) k-points grid generated automatically using the Monkhorst–Pack method[27] for the relaxation calculations. Complete linear synchronous transit (LST)/quadratic synchronous transit (QST) calculations were performed to locate transition states (TS) in Dmol[3] code. It is found that all the minima possess real frequencies, and the transition states have only one imaginary frequency. Additionally, the contributions of the long-range dispersion correction *via* Tkatchenko and Scheffler's scheme are also tested, and we found that the long-range dispersion correction yields essentially different adsorption energies (increased by 0.05~0.18 eV), while its influence on the energy barriers and the reaction energies are negligible.

The calculated lattice constant of h-BN is 2.51 Å with the B-N bond of 1.45 Å, which is in good agreement with the previous study[21]. The BN support is modeled by a 4×4 h-BN supercell with a vacuum layer of 15 Å. The test calculations suggest that the current model is enough to reveal the CO oxidation process. The adsorption energy (E_{ads}) is defined as $E_{ads} = E_{adsorbate} + E_{support} - E_{adsorbate/support}$, where $E_{adsorbate}$, $E_{support}$ and $E_{adsorbate/support}$ are the total energies of the free adsorbate, the corresponding support and the support with the adsorbate, respectively. All three types of energy were derived from the calculations using the same periodic box dimensions and the same calculated setting. With this definition, a positive value indicates an exothermic adsorption.

3. Results and Discussion

3.1 Single Pd atom on h-BN

For the h-BN support, there are three typical configurations, defect-free h-BN, N-defect h-BN (N_V/BN) and B-defect h-BN (B_V/BN). Firstly, the adsorption of single Pd atom on defect-free h-BN has been explored with the various initial structures, and there are two stable adsorption configurations found with Pd atom on the top of nitride atom and on the hollow site of hexagonal ring, respectively, as shown in Figure 1a and 1b. The distances of the Pd adatom to the BN support are about 2.16 Å and 2.12 Å, respectively, and the negligible distortion has been found for the BN support by the Pd adsorption. The calculated adsorption energies are 0.79 and 0.59 eV, respectively, both of which are much smaller than the binding energy of Pd dimer (1.19 eV) and Pd bulk (3.89 eV). This indicates that the Pd atoms prefer to cluster on the defect-free h-BN monolayer.

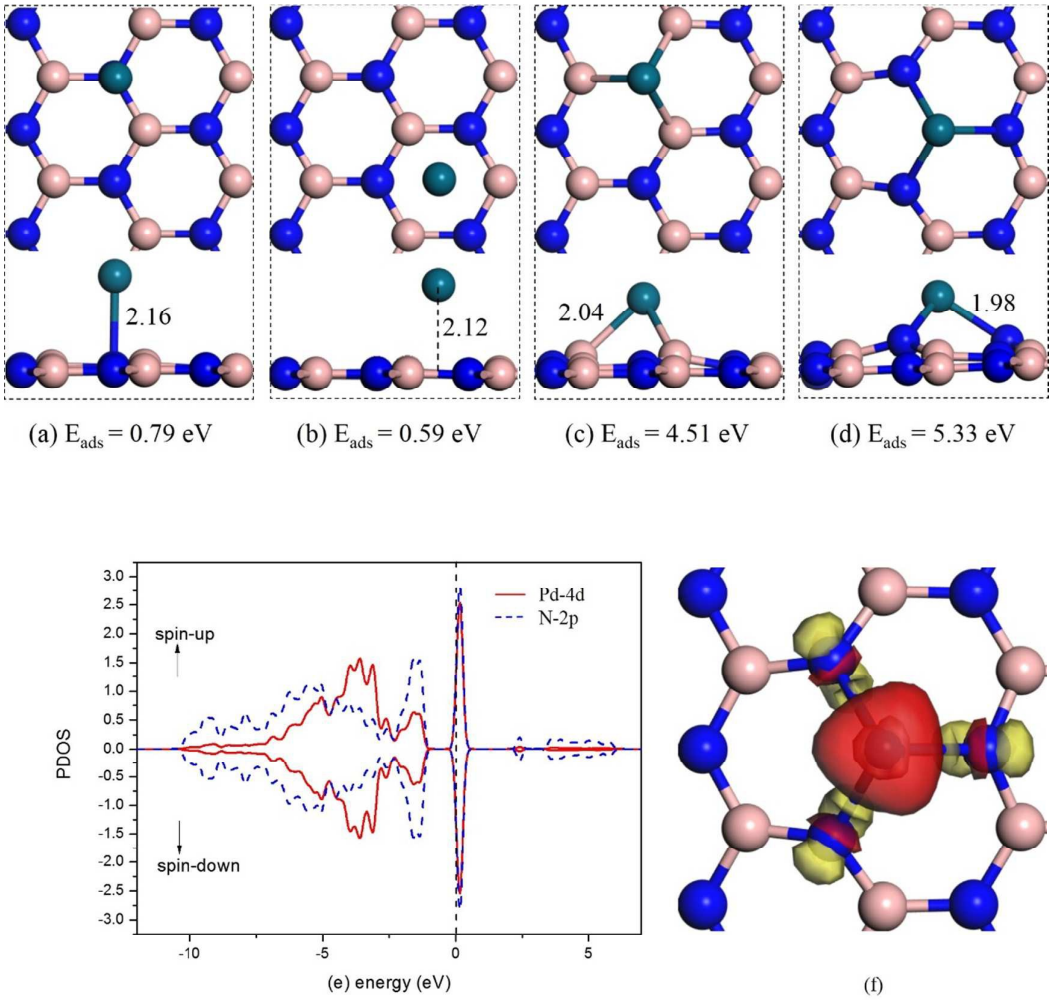

Figure 1. Top and side views of the most stable configurations of Pd adsorbed on (a) nitride site, (b) hollow site, (c) nitride and (d) boron defect supports, respectively. (e) the spin-polarized partial density of states (PDOS) projected on Pd-4d (red) and N-2p (blue) states. The Fermi level is set to zero. (f) the charge difference density between the single Pd atom and the B_V-BN. For the contour plots, the charge accumulation regions are rendered in yellow while the charge deplete regions are shown in red. The contour value of the charge difference density is ± 0.05 a.u. Hereafter, the pink, blue, and bice spheres represent B, N and Pd, respectively. And the bond distances are in angstroms.

For the defect h-BN, we consider both the N-defect and B-defect h-BN as supports to anchor the single Pd atom from the various initial structures[28]. Their most stable configurations are presented in Figure 1c and 1d, and marked as Pd_1-N_V/BN and Pd_1-B_V/BN, respectively. Upon staying on the defect-BN, the formed Pd-B and Pd-N bonds secure the single Pd atom with the bond length of 2.04 Å and 1.98 Å, respectively. The corresponding adsorption energies are 4.51 eV and 5.33 eV, respectively, both of which are larger than the binding energy of Pd dimer (1.19 eV) and Pd bulk (3.89 eV). This indicates that both

defect-BN configurations provide stable anchoring sites for the single Pd atom. The B-defect is more popular than the N-defect in BN, according to the calculated formation energies[29] and the fact that the boron monovacancy is preferably fabricated by the high energy charged electrons in experiment[30]. Thus, the Pd_1-B_V/BN configuration would be more preferable than the Pd_1-N_V/BN configuration, and the former will be focused on in the following.

To gain a deeper insight into the properties of the Pd_1-B_V/BN configuration, we perform the electronic structure analysis of the partial density of states (PDOS) and the Mulliken charge population analysis. The DOS curves are presented in Figure 1e, and there are many overlapped peaks between the Pd-4d states and the N-2p states, indicating the hybridization between Pd-4d states and N-2p states, resulting in the strong interaction of the Pd and its three neighbor N atoms. Moreover, there are four sharp peaks (two from Pd-4d states and the other two from N-2p states) across the Fermi level (E_F), suggesting the high activity of the Pd_1-B_V/BN system. As indicated by the charge density difference (Figure 1f), there is charge transfer from Pd atom to B_V/BN support, and the transferred charge is mainly localized on the three neighbor N atoms of Pd adatom. The Mulliken charge analysis shows the charge transfer from Pd atom to B_V/BN support is 0.19 |e|.

As a catalyst, the stability of single atomic Pd adsorbed on B_V/BN is greatly important. Here, we investigate the mobility of the single Pd atom to reveal the stability of the Pd_1-B_V/BN system, and we take the most stable adsorption site as the initial states (IS), and the other two stable ones as the final states (FS1 and FS2, respectively). The calculated mobility barrier of the Pd atom from IS to FS1 and FS2 are 3.77 eV and 5.26 eV, respectively (see Figure 2). The large diffusion barriers indicate the immobility of the single Pd atom on the B-defect h-BN. The immobility of the single Pd atom together with its strong adsorption energy (compared to the binding energy of Pd dimer and bulk) implies that the metal clustering of Pd atom would be rather difficult and the Pd_1-B_V/BN configuration is extraordinarily stable, which might bear higher temperatures under standard conditions.

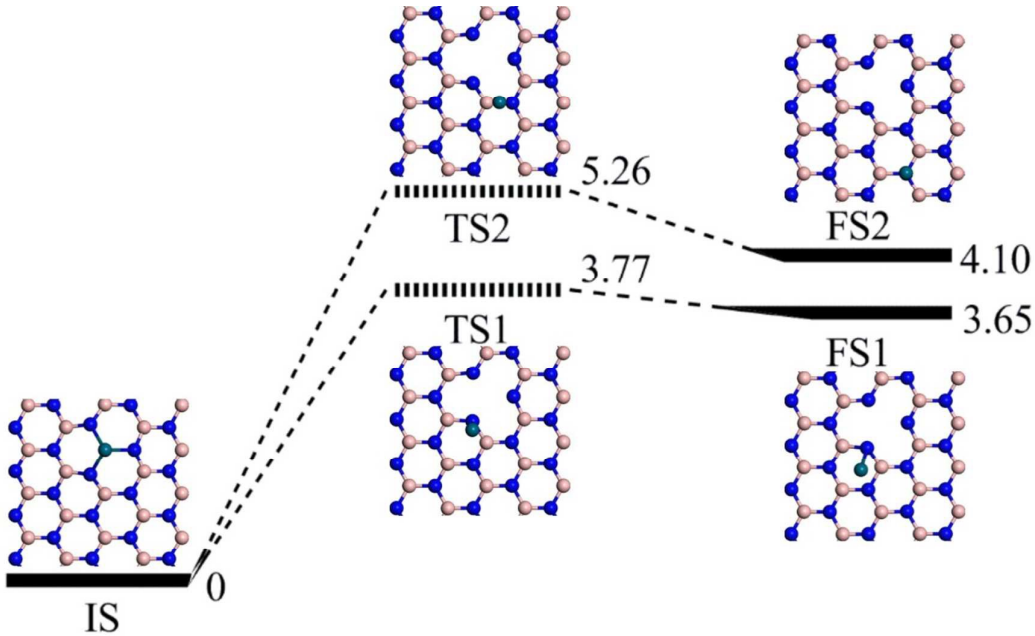

Figure 2. The reaction profiles of diffusion of single Pd atom from its most stable adsorption site to the other stable adsorption sites.

3.2 Adsorption of O_2, CO, O, and CO_2 on Pd_1-B_V/BN

Before investigating the CO oxidation reaction, we firstly study the adsorption of various species involved in CO oxidation on the Pd_1-B_V/BN, including O_2, CO, O, and CO_2. Various initial adsorption configurations have been considered to obtain the most stable ones, which are summarized in Figure 3. It is found that all the species prefer to stay on the Pd site but not the BN support.

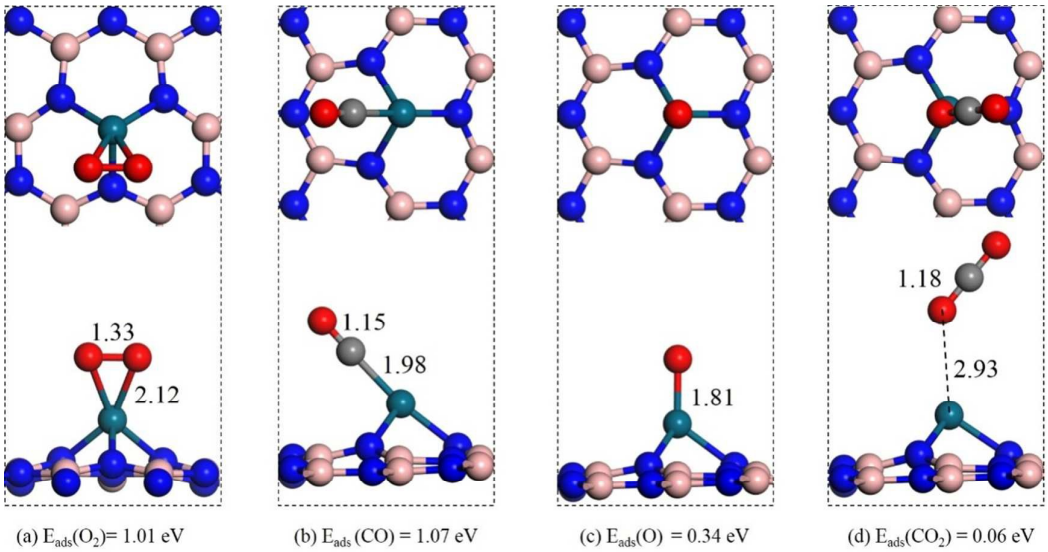

Figure 3. Top and side views of the most stable adsorption configurations of (a) O_2, (b) CO, (c) O, and (d) CO_2 on Pd_1-B_V/BN. Hereafter, the red and gray spheres represent O and C

atoms, respectively.

The adsorbed O_2 molecule anchors on Pd adatom and prefers to lie parallel to the h-BN support, and the O-O bond is enlarged from 1.23 Å to 1.33 Å with the two Pd-O bonds of 2.12 Å formed. The calculated adsorption energy is 1.01 eV. According to the Mulliken charge analysis, the adsorbed O_2 is negatively charged by 0.34 |e|, and the single Pd adatom is positively charged by 0.28 |e|, indicating the key role of the Pd atom to activating the adsorbed O_2. Figure 4 presents the PDOS curves of the related systems of the O_2 and CO adsorption on Pd_1-B_V/BN. Upon O_2 adsorption, the curve of Pd-4d states are broadened, and there are two new hole peaks appearing above the Fermi level to overlap with $2\pi^*$ of orbitals of O_2. At the energy area of -7.5 eV to -5.0 eV, there are three peaks of the 1π orbitals of adsorbed O_2, and the three peaks well overlap with the three peaks of the Pd-4d states, implying the strong hybridization between the Pd-4d states and the 2p states of the adsorbed O_2. The elongation of the O-O bond, the great charge transfer and the strong hybridization of the Pd-4d states and O-2p states suggest that the O_2 is significantly activated.

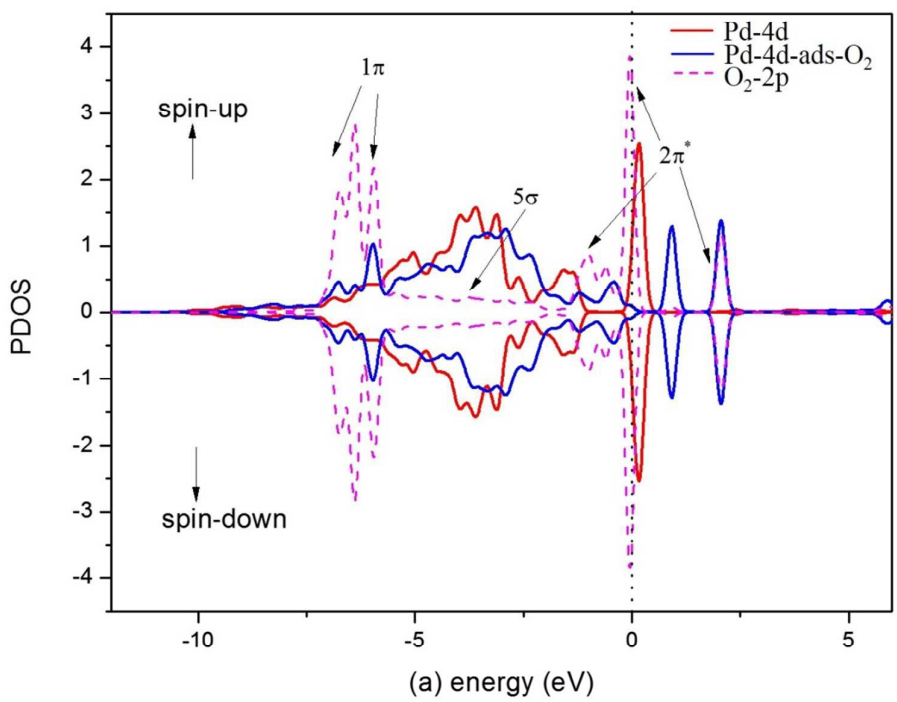

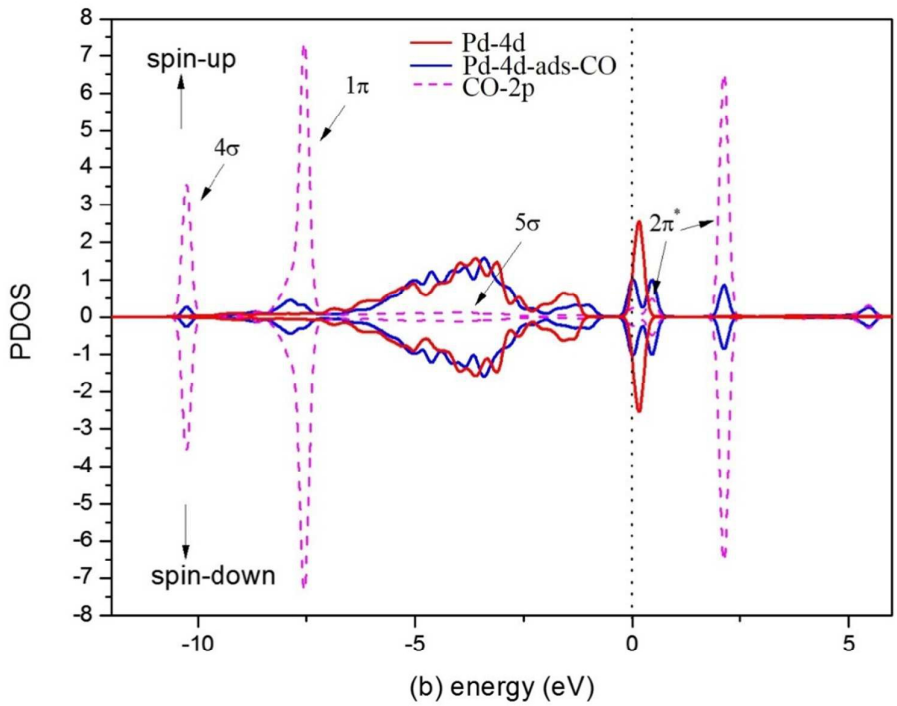

Figure 4. PDOS for (a) O_2 and (b) CO on Pd_1-B_V/BN. The red (blue) curves represent the PDOS of Pd-4d states without (with) O_2 or CO adsorption and the Magenta red dash curves represent the PDOS of the 2p states of the absorbate (O_2 or CO).The Fermi level was set to zero.

The most stable CO adsorption configuration is presented in Figure 3b and the CO is tilted to the Pd_1-B_V/BN plane with the C-O bond of 1.15 Å (similar to the gas CO), and the C-Pd bond of 1.91 Å. The calculated adsorption energy is 1.07 eV, which is only 0.06 eV more favorable than that for O_2 adsorption, suggesting that the adsorption of CO is slightly preferred. The Mulliken charge analysis shows that the adsorbed CO is positively charged by 0.26 |e| and the Pd accepts 0.25 |e| while the changes of boron and nitride atoms charges are negligible, indicating the CO and the Pd act as a charge donor and acceptor respectively. As shown in Figure 4b, upon CO adsorption, Pd-4d states split into two peaks near the Fermi level, and the two peaks strongly hybridize with the $2\pi^*$ orbitals of the absorbed CO. In the energy area of -12 eV to -7 eV, the 4σ and 1π orbitals of CO are also hybridized with the Pd-4d states. The strong hybridization between CO and Pd is in line with the strong interaction between Pd and CO.

The most stable adsorption structure of single O atom on Pd_1-B_V/BN is presented in Figure 3c. Compared with that of O_2 adsorption (Figure 3a), the adsorption energy of the O atom is reduced to 0.34 eV and the O-Pd bond is reduced to 1.81 Å. The adsorbed O atom is negatively charged by 0.48 |e| [about half of $q(O^{2-})$] [31], indicating the formation of the O^- species. The O^- species is believed to be more reactive than O^{2-} [32]. As presented below, the O^-

species have great activity to oxidize the CO.

As the final product of CO oxidation, only the physical adsorption configuration is found for the CO_2 adsorption (Figure 3d), with a rather small adsorption energy of 0.06 eV and a long Pd-O distance of 2.93 Å. The rather weak interaction (the small adsorption energy) together with the negligible charge transfer between the CO_2 and support indicates that the formed CO_2 species would be spontaneously released at room temperature.

3.3 CO oxidation on Pd_1-B_V/BN

Generally, the normal reaction mechanisms of the CO oxidation are the ER mechanism and LH mechanism[33]. The carbonate-like (CO_3) and peroxide-like complex (OCOO) are the essential intermediates for CO oxidation *via* ER and LH mechanisms, respectively. For the ER mechanism, the gas-phase CO molecules directly react with the activated O_2 to form the carbonate-like intermediate or CO_2. And the LH mechanism involves the co-adsorption of O_2 and CO molecules, the formation of a peroxide-like intermediate complex and desorption of CO_2 molecule.

Interestingly, there are two new CO oxidation mechanisms, named as termolecular Eley–Rideal mechanism (TER) found by Yang et al.[11] and termolecular Langmuir–Hinshelwood mechanism (TLH) found by Zeng et al.[34]. In the TER mechanism, a free O_2 molecule is activated by two co-adsorbed CO molecules to form an OCO-metal-OCO intermediate, which is a pentagonal ring structure, and the intermediate configuration would dissociate into two CO_2 molecules synchronously. And in the TLH mechanism, the initial state is the configuration that one O_2 molecule and two CO molecules are co-adsorbed on catalyst. The presence of the OCOPdOCO intermediate and the co-adsorption configuration of two CO molecules (as presented below) on the Pd_1-B_V/BN support implies the probability of the TER mechanism for CO oxidation. However, the absence of the co-adsorption configuration of one O_2 and two CO molecules suggests that the TLH mechanism is not applicable for CO oxidation on Pd_1-B_V/BN system. Furthermore, the co-adsorption configuration of three CO molecules is also taken into consideration, and it is found that the Pd_1-B_V/BN can't chemisorb a third CO, which avoids the CO poisoning problem[20] and provides the possibility of CO oxidation through the ER, LH and TER mechanism.

3.3.1 *ER mechanism*

The reaction profiles of the ER mechanism are presented in Figure 5, including the involved co-adsorption configurations and the transition states (TS). In Figure 5, the physisorption configuration of CO above the pre-adsorbed O_2 on Pd_1-B_V/BN is selected as the initial state (IS). When approaching the activated O_2, CO binds to O_2 with the breakage of the O-O bond and the formation of the new C-O bonds to form a carbonate-like intermediate state (MS) *via* the energy barrier of 1.21 eV and exothermic reaction energy of 3.70 eV (the reaction energy is defined as the change in the total energies between reactants and products). Subsequently, the carbonate-like structure dissociates by cleavage of one of C-O bonds *via* the reaction energy barrier of 1.29 eV and endothermic reaction energy of 0.98 eV, resulting in the formation of a CO_2 and an atomic O atom on the Pd_1-B_V/BN. The calculated adsorption

energy of CO_2 on the Pd_1-B_V/BN with the adsorption of atomic O is 0.10 eV, and the CO_2 is as far as 2.93 Å to the adsorbed atomic O. Due to the rather weak adsorption and the long distance to the support, the formed CO_2 will be spontaneously released as the free CO_2 at room temperature. *Summarily*, the rate-limiting step of the current ER mechanism is the formation of the CO_2 from carbonate-like structure with the cleavage of one of C-O bonds, with the corresponding reaction energy barrier of 1.29 eV and endothermic reaction energy of 0.98 eV.

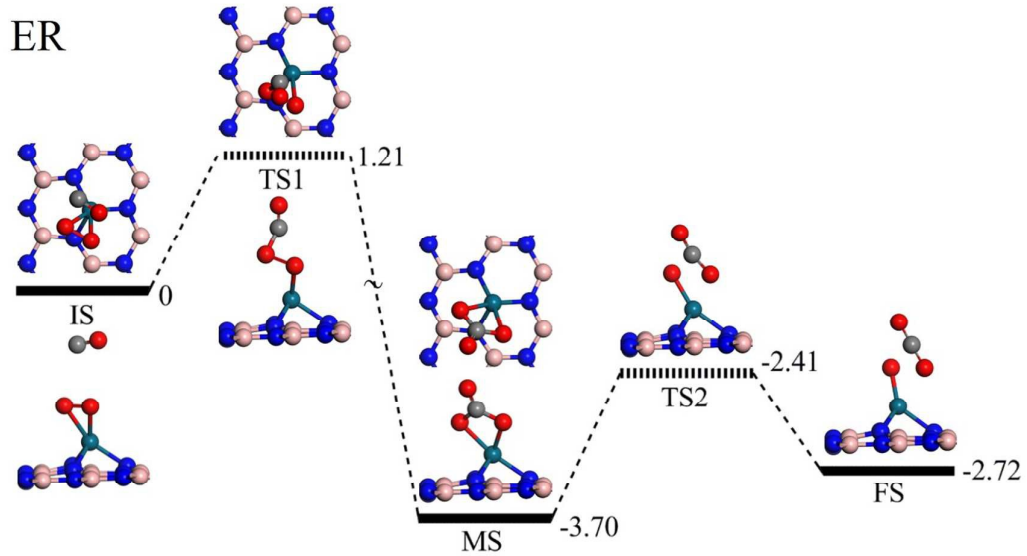

Figure 5. The reaction profiles of CO oxidation *via* the ER mechanism. Hereafter, the local configurations of the adsorbates on Pd_1-B_V/BN at initial states (IS), transition states (TS), intermediate states (MS) and final states (FS) along the minimum-energy pathway are shown in the inserts, respectively.

Given that the adsorption energies of CO and O_2 are both lower (~0.2 eV) than the reaction barrier of the formation of carbonate-like structure, the desorption of adsorbed CO and O_2 would be slightly preferable rather than the formation of carbonate-like structure. This indicates that the CO oxidation over Pd_1-B_V/BN *via* the ER mechanism is not preferable, which is similar to that of CO oxidation on the Cu embedded in h-BN *via* the ER mechanism[19]. Therefore, the LH and TER mechanism will be emphasized in the following. The oxidation of the second CO by the left atomic O on Pd_1-B_V/BN will be presented in the next subsection.

3.3.2 *LH mechanism*

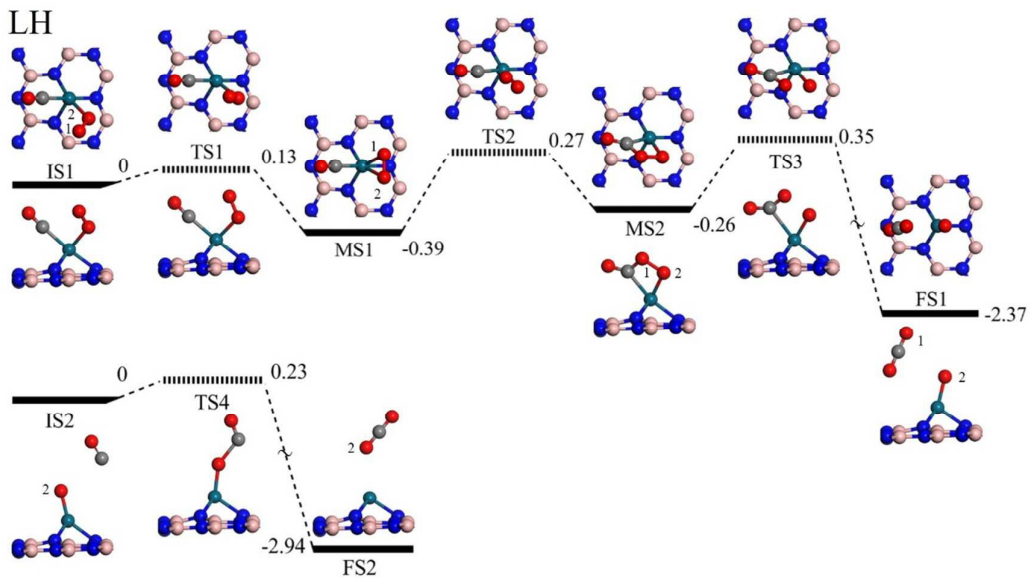

Figure 6. The reaction profiles of CO oxidation *via* the LH mechanism. The two O atom of O_2 molecule are marked as O1 and O2, respectively.

Figure 6 displays the reaction pathway of CO oxidation *via* the LH mechanism. Different from ER mechanism, the co-adsorbed CO and O_2 will react to form a peroxide-like intermediate. As the initial state (IS1), the co-adsorption energy of CO and O_2 is 1.34 eV, in which only one oxygen atom (O2) of the O_2 molecule binds to the Pd atom. And the co-adsorption energy is larger than those of the isolated CO (1.07 eV) and O_2 (1.01 eV), indicating the enhancement of the co-adsorption of CO and O_2. When CO and O_2 are co-adsorbed on Pd_1-B_V/BN, one of the O atom (O1) in the adsorbed O_2 molecule starts to approach the Pd atom to form a more stable co-adsorption configuration (MS1), in which the two oxygen atoms of the O_2 molecule both bind to the Pd atom with the Pd-O bonds of 2.16 Å and the co-adsorption energy of CO and O_2 is 1.73 eV. The corresponding energy barrier and exothermic reaction energy are 0.13 eV and 0.39 eV, respectively. Subsequently, the O1 atom will approach the carbon atom of CO to form one OCOO intermediate (MS2), in which the O1-O2 bond is enlarged to 1.47 Å, while the O1-C bond is decreased to 1.35 Å. The corresponding reaction barriers is 0.66 eV, whereas the reaction is endothermic (0.13 eV).

Upon the cleavage of the O-O bond of the oxygen molecule, there is a CO_2 molecule formed, and the corresponding reaction energy barrier and exothermic reaction energy is 0.61 eV and 2.11 eV, respectively. Similarly, due to its rather weak adsorption and the long distance to the support, the formed CO_2 will be spontaneously released as a free CO_2 at room temperature.

Upon the release of the formed CO_2, there is an atomic O left on the Pd_1-B_V/BN with the Pd-O bond of 1.81 Å. It is found that the left atomic O is negatively charged by 0.48 |e| [about half of $q(O^{2-})$], implying the formation of the O^- species[31]. The O^- species is believed to be more reactive than O^{2-} [32], and ready to oxidize the (second) CO. The (2nd) CO is firstly

physically adsorbed on the left atomic O, with the C-O distance of 3.03 Å. When the CO approaches the left O to form the second CO_2 molecule *via* the reaction energy barrier and exothermic reaction energy of 0.23 eV and 2.94 eV, respectively. The adsorption of the formed CO_2 is rather weak (0.06 eV), suggesting that the formed CO_2 species would be released spontaneously and Pd_1-B_V/BN system is refreshed and ready for a new cycle of CO oxidation.

Summarily, the corresponding rate-limiting step is TS2 (0.66 eV) with the formation of the OCOO intermediate, which is endothermic (0.13 eV). In the LH mechanism, the reaction energy of the entire reaction process from the co-adsorption of O_2 and CO to the formation of the first CO_2 is exothermic (2.37 eV), and it can compensate for the small endothermic reaction energy of the rate-limiting step (0.13 eV). In addition, the final product in FS2, CO_2, has the weak adsorption on Pd_1-B_V/BN catalyst and it will be easily desorbed, suggesting the concentration of reactants (CO and O_2) is higher than the product (CO_2). All these results indicate that the CO oxidation reaction *via* the LH mechanism is hardly inhibited by the step from MS1 to MS2 and the chemical equilibrium will shift to the formation of the product CO_2.

3.3.3 *TER mechanism*

As mentioned above, a new mechanism for CO oxidation named as TER mechanism[11] is reported on the single Au atom supported by h-BN. In the TER mechanism, a free O_2 molecule is activated by two co-adsorbed CO molecules to form an OCO-metal-OCO intermediate. Here, we take the co-adsorption configuration of two CO molecules as the first stage of the TER mechanism. The reaction profiles of the TER mechanism are presented in Figure 7, including the involved co-adsorption configurations, the transition states (TS) and the important intermediate (OCOPdOCO).

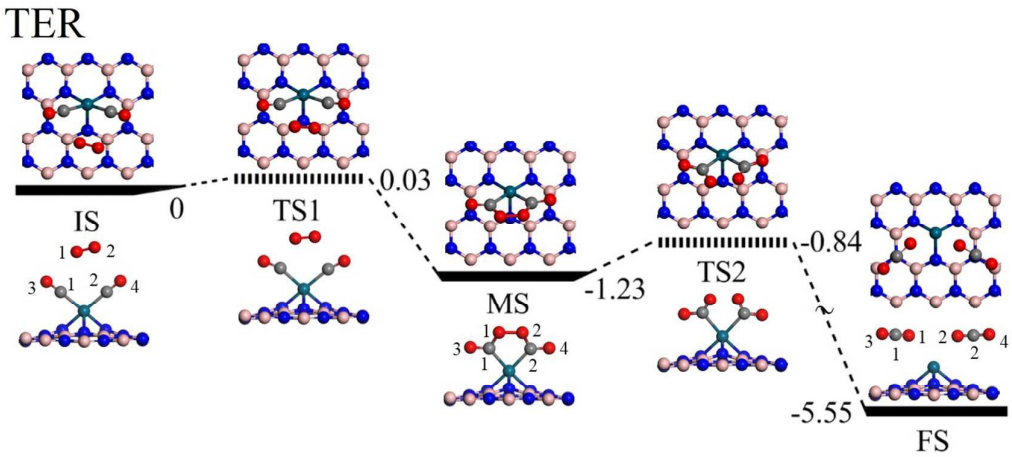

Figure 7. The reaction profiles of CO oxidation *via* the TER mechanism. The two O atoms of O_2 molecule are marked as O1 and O_2, and the C and O atom of two CO molecules

are marked as C1, C2, O3 and O4, respectively.

For the configuration of two CO molecules co-adsorbed on Pd_1-B_V/BN, the adsorption energy of the second CO is 0.77 eV and the co-adsorption energy is 1.84 eV. In the reported TER mechanism of the CO oxidation on the Au-BN system, the two adsorbed CO molecules would promote the activation of the O_2 molecule, *i.e.* O_2 molecule is activated by CO molecules directly[11]. Indeed, we also found the activation of the O_2 is promoted by the two pre-adsorbed CO molecules on the Pd_1-B_V/BN. As the initial state, two CO molecules are chemically co-adsorbed on Pd atom with one physically adsorbed O_2 molecule, where the distances of O1-C1 and O2-C2 are 3.46 Å and 3.78 Å, respectively, and the angle of C1-Pd-C2 is 95.08°. The physically adsorbed O_2 molecule firstly approaches the two carbon atoms simultaneously v*ia* a rather small reaction energy barrier of 0.03 eV to form the OCOPdOCO intermediate, and the corresponding (exothermic) reaction energy is 1.23 eV. The formed OCOPdOCO intermediate has the pentagonal ring structure (see the "MS" of Figure 7), in which the O-O bond is enlarged to 1.49 Å. Subsequently, the OCOPdOCO intermediate dissociates to form two adsorbed CO_2 molecules with the cleavage of the O-O bond *via* TS2, and the corresponding reaction energy barrier and (exothermic) reaction energy are 0.39 eV and 4.32 eV, respectively. Moreover, the adsorption energies of the formed CO_2 molecules are rather small (~0.16 eV), suggesting that the formed CO_2 molecules would be released spontaneously and the Pd_1-B_V/BN system is refreshed and ready to a new cycle of CO oxidation.

Summarily, in the current TER mechanism, the rate-limiting step is the formation of the two CO_2 molecules from the dissociation of the OCOPdOCO intermediate with the small reaction energy barrier of 0.39 eV. This indicates the great activity of the Pd_1-B_V/BN for CO oxidation, which is mainly attributed to the "CO-Promoted O_2 Activation"[11]. The positively charged carbon atoms of the CO molecules, which would be the good anchor for the negatively charged O_2. The energy barrier of the rate-limiting step for TER is dramatically lower than that for LH mechanism (0.39 eV *vs* 0.66 eV), indicating that the TER mechanism (CO-Promoted O_2 Activation) would be more preferable than the LH mechanism. According to the initial stage of LH (CO and O_2) and TER mechanism (2CO), when firstly loading one reactant (O_2) at a time, beginning with the co-adsorption of O_2 and CO followed by the formation of OCOO intermediate, the LH mechanism will take place. On the contrary, when firstly loading another reactant (CO) at a time, beginning with the co-adsorption of two CO followed by the formation of OCOPdOCO intermediate, the TER mechanism will take place. However, it is quite impractical to feed two reactants one-by-one. In order to improve the reaction activity by the most preferable mechanism (TER), the concentration of the CO should dominate over the O_2 in their mixed feed. The high-loading of CO will occupy the Pd site and can not only adsorb on the bare Pd_1-B_V/BN catalyst improving the reaction rate in the stepwise pathway *via* the preferable TER mechanism, but also eliminate the co-adsorption of CO and O_2 on Pd_1-B_V/BN *via* the LH mechanism.

4. Conclusion

The electronic structure analysis and the mechanisms of CO catalytic oxidation to CO_2 on Pd_1-B_V/BN are studied by DFT-D calculations, systematically. Specifically, we calculate the diffusion barrier of single Pd atom on B_V/BN to reveal the stability of the Pd_1-B_V/BN system. It is found that the metal clustering of Pd atom would be excluded and the Pd_1-B_V/BN system is dramatically steady.

Summarizing our calculated reaction energy barriers for all of the CO oxidation mechanisms (ER, LH, TER), it is concluded that the traditional mechanism (LH) and the new mechanism (TER) are both preferable for CO oxidation on Pd_1-B_V/BN under experimental conditions because of the high reaction energy barrier of the rate-limiting step in ER mechanism. The rate-limiting steps for the preferable LH and TER mechanisms are the formation of the OCOO intermediate and the formation of the two CO_2 molecules from the dissociation of the OCOPdOCO intermediate, respectively and the corresponding reaction barriers of the rate-limiting steps for the two mechanisms are 0.66 eV and 0.39 eV, respectively. Given the relatively small energy barriers for LH and TER (0.66 eV and 0.39 eV, respectively), we believe that both two mechanisms are possible and could happen at the low temperature. Also, the energy barrier of the rate-limiting step for TER is dramatically lower than that for LH mechanism (0.39 eV *vs* 0.66 eV), indicating that the TER mechanism (CO-Promoted O_2 Activation) would be more preferable than the LH mechanism.

Utilization of the novel properties of SACs seems to provide vast opportunities for their applications in heterogeneous catalysis. The current study will help to understand the various mechanisms of the CO oxidation and shed light on the design of the CO oxidation catalyst based on the single metal atom concept to lower CO emissions and solve the growing environment problem. With the establishment of SACs as a new concept and a thorough elucidation of the nature of single atom catalysis, we believe that the development and understanding of SACs might be a new frontier in heterogeneous catalysis.

Acknowledgements

This work is supported by the National Natural Science Foundation of China (Grant Nos. 51401078, and 11147006), and sponsored by Program for Science & Technology Innovation Talents in Universities of Henan Province (Grant No. 15HASTIT016). Doctor C. He also acknowledges the support from the Henan Joint Funds of the National Natural Science Foundation of China (Grant Nos. U1404216, and U1504108), and the Natural Science Foundation of Nanyang Normal University (Nos. ZX2014088, and QN2015020). We are grateful to Computing Center of Jilin Province for essential support.

Refs

1. Z.-P. Liu, P. Hu and A. Alavi, *J. Am. Chem. Soc.*, 2002, **124**: 14770.
2. K. Bleakley and P. Hu, *J. Am. Chem. Soc.*, 1999, **121**: 7644.
3. A. Eichler, *Surf. Sci.*, 2002, **498**: 314.
4. X.-Q. Gong, Z.-P. Liu, R. Raval and P. Hu, *J. Am. Chem. Soc.*, 2004, **126**: 8.
5. J. M. Thomas, R. Raja and D. W. Lewis, *Angew. Chem. Int. Edit.*, 2005, **44**: 6456.
6. B. Qiao, A. Wang, X. Yang, L. F. Allard, Z. Jiang, Y. Cui, J. Liu, J. Li and T. Zhang, *Nat. Chem.*, 2011, **3**: 634.
7. S. Sun, G. Zhang, N. Gauquelin, N. Chen, J. Zhou, S. Yang, W. Chen, X. Meng, D. Geng and M. N. Banis, *Sci. Rep.*, 2013, **3**: 1775.
8. X. Zhang, J. Guo, P. Guan, C. Liu, H. Huang, F. Xue, X. Dong, S. J. Pennycook and M. F. Chisholm, *Nat. Commun.*, 2013, **4**: 1924.
9. A. Uzun, V. Ortalan, N. D. Browning and B. C. Gates, *J. Catal.*, 2010, **269**: 318.
10. X.-F. Yang, A. Wang, B. Qiao, J. Li, J. Liu and T. Zhang, *Acc. Chem. Res.*, 2013, **46**: 1740.
11. K. Mao, L. Li, W. Zhang, Y. Pei, X. C. Zeng, X. Wu and J. Yang, *Sci. Rep.*, 2014, **4**: 5441.
12. C. Huang, X. Ye, C. Chen, S. Lin and D. Xie, *Comput. Theor. Chem.*, 2013, **1011**: 5.
13. Y. Li, Z. Zhou, G. Yu, W. Chen and Z. Chen, *J. Phys. Chem. C*, 2010, **114**: 6250.
14. Y.-H. Lu, M. Zhou, C. Zhang and Y.-P. Feng, *J. Phys. Chem. C*, 2009, **113**: 20156.
15. X. Liu, Y. Sui, T. Duan, C. Meng and Y. Han, *Phys. Chem. Chem. Phys.*, 2014, **16**: 23584.
16. Y. Tang, Z. Yang and X. Dai, *Phys. Chem. Chem. Phys.*, 2012, **14**: 16566.
17. E. H. Song, Z. Wen and Q. Jiang, *J. Phys. Chem. C*, 2011, **115**: 3678.
18. S. Lin, X. Ye, R. S. Johnson and H. Guo, *J. Phys. Chem. C*, 2013, **117**: 17319.
19. X. Liu, T. Duan, Y. Sui, C. Meng and Y. Han, *RSC Advances*, 2014, **4**: 38750.
20. X. Liu, T. Duan, C. Meng and Y. Han, *RSC Advances*, 2015, **5**: 10452.
21. P. Zhao, Y. Su, Y. Zhang, S.-J. Li and G. Chen, *Chem. Phys. Lett.*, 2011, **515**: 159.
22. D. Palagin and J. P. K. Doye, *Phys. Chem. Chem. Phys.*, 2015, **Advance Article: 10.1039/C5CP00889A**.
23. Y. Zhou, Z. Wang and C. Liu, *Catal. Sci. Technol.*, 2015, **5**: 69.
24. B. Delley, *Phys. Rev. B*, 2002, **66**: 155125.
25. J. P. Perdew, K. Burke and M. Ernzerhof, *Phys. Rev. Lett.*, 1996, **77**: 3865.
26. A. Tkatchenko and M. Scheffler, *Phys. Rev. Lett.*, 2009, **102**: 073005.
27. H. J. Monkhorst and J. D. Pack, *Phys. Rev. B*, 1976, **13**: 5188.
28. A. Zobelli, A. Gloter, C. Ewels, G. Seifert and C. Colliex, *Phys. Rev. B*, 2007, **75**: 245402.
29. A. Du, Y. Chen, Z. Zhu, R. Amal, G. Q. Lu and S. C. Smith, *J. Am. Chem. Soc.*, 2009, **131**: 17354.
30. C. Jin, F. Lin, K. Suenaga and S. Iijima, *Phys. Rev. Lett.*, 2009, **102**: 195505.
31. Z. Lu, D. Ma, L. Yang, X. Wang, G. Xu and Z. Yang, *Phys. Chem. Chem. Phys.*, 2014, **16**: 12488.
32. I. Kocemba and J. M. Rynkowski, *Catal. Today*, 2011, **169**: 192.
33. K. J. Laidler, *Pure. Appl. Chem.*, 1996, **68**: 149.
34. C. Liu, Y. Tan, S. Lin, H. Li, X. Wu, L. Li, Y. Pei and X. C. Zeng, *J. Am. Chem. Soc.*, 2013, **135**: 2583.